Compartmentalization of second messengers in neurons: A mathematical analysis

Wen Chen, Herbert Levine, and Wouter-Jan Rappel
Center for Theoretical Biological Physics and Department of Physics, University of California–San Diego, La Jolla, California 92093-0319, USA

(Received 26 June 2009; published 2 October 2009)

Recent experiments in hippocampal neurons have demonstrated the existence of compartments with elevated levels of second messenger molecules such as cyclic AMP. This compartmentalization is believed to be necessary to ensure downstream signaling specificity. Here we use analytical and numerical techniques to investigate the diffusion of a second messenger in the soma and in the dendrite of a neuron. We obtain analytical solutions for the diffusion field and examine the limit in which the width of the dendrite is much smaller than the radius of the soma. We find that the concentration profile depends both on the degradation rate and the width of the dendrite and that compartmentalization can be indeed be achieved for small width to soma radius ratio.

DOI: 10.1103/PhysRevE.80.041901 PACS number(s): 87.10.Ca, 87.15.Vv, 87.16.A−

I. INTRODUCTION

A large variety of cellular processes are regulated by the diffusible second messenger cyclic adenosine monophosphate (cAMP). This messenger is generated by membrane bound adenylyl cyclases (ACs) which, in turn, are activated by external signals. cAMP is degraded by phosphodiesterases (PDEs), which can be localized to specific cell locations or can be diffusible. The fact that cAMP is able to activate multiple pathways raises the question of signal specificity: how can one avoid the activation of undesirable pathways following the input to a specific pathway? One way to achieve signaling specificity is to have cAMP levels that are elevated in small spatial compartments but remain low in the rest of the cell. Indeed, an increasing number of experiments had shown that there exist cAMP microdomains in several different cell types, including cardiac myocytes [1,2], kidney cells [3], and neurons [4].

This compartmentalization is surprising since cAMP is a small hydrophilic molecule, which diffuses very fast with a diffusion constant of $D=100\sim700\ \mu\mathrm{m}^2/\mathrm{s}$. Thus, with no restriction on diffusion, AC activation will quickly lead to an increase in the global cAMP level. To prevent the indiscriminate activation of multiple pathways, there needs to be a mechanism that restricts the diffusion away from the microdomain. Possible mechanisms to create compartments with elevated levels of cAMP include physical barriers, including cell membranes and intercellular structures, and nonuniform degradation. An example of the latter mechanism was suggested for myocytes where physical barriers appear not to play a significant role. In this mechanism, cross-talk is avoided by colocalizing the final targets of the signaling pathway with the ACs and by spatially separating the source of cAMP from regions with an elevated PDE concentration. In our previous work, we constructed a mathematical model to investigate the viability of this mechanism. Using an analytical approach, we derived expressions for the steady-state cAMP concentration field and found conditions for which this mechanism can lead to signal specificity [5].

Here, we will again examine second messenger compartmentalization using analytical techniques but will now focus on the cAMP concentration profiles in neurons. We are motivated by recent experiments in rat hippocampal slices [6] which demonstrated that, after stimulation, cAMP accumulates preferentially at the distal dendrites and that the soma maintains a low level of cAMP. Thus, sharp gradients of cAMP exist at the junction between the dendrites and the soma and it was suggested that the two domains with sharply different cAMP concentrations ensure signal specificity.

Using a simple representation of the cell geometry, we will present asymptotic analytical solutions that quantify how cell shape and degradation rates affect the spatial cAMP concentration profiles. This will be done both in two dimension and three dimension (3D), the latter assuming axial symmetry; for ease of presentation, we have placed the 3D results in Appendix B. Our model does not consider downstream pathways, such as protein kinase A (PKA), but is able to capture the salient ingredients required for second messenger compartmentalization. Our main result, in agreement with the numerical findings of Neves *et al.* [6], is that a sharp cAMP gradient between the soma and the dendrite requires a minimum level of signal degradation. Furthermore, we find that the cAMP gradient at the junction depends critically on the width of the dendrite.

II. MODEL

As in the numerical work of Neves *et al.* [6], we assume a neuron with the simplified geometry shown in Fig. 1. It consists of a circle with radius R, representing the cell body, and a protruding rectangle with length L and half width w, representing the dendrite. The 3D version, where the rectangle is replaced by a right circular cylinder, is presented in Appendix B. Since the width of the dendrite is much smaller than the radius of the soma, i.e., $w \ll R$, we can approximate the connecting part of the circle and the rectangle to be a straight line. Thus, we have

$$w = R \sin\theta_0 \simeq R\theta_0, \tag{1}$$

where θ_0 is defined in Fig. 1. Note that the surface-to-volume ratio for the dendrite is much larger than for the soma.

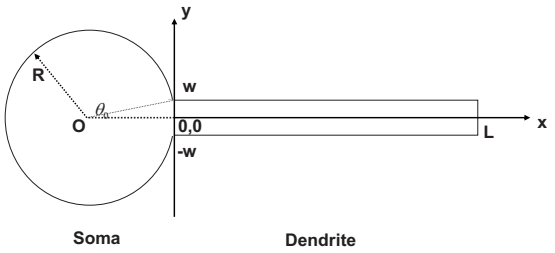

FIG. 1. The geometry considered in this paper. The circle with radius R represents the soma, and the rectangle with length L and half width w represents the dendrite. The sources for the second messengers are uniformly distributed on the perimeter, and the degradation molecules are uniformly distributed in both the soma and the dendrite.

For simplicity, we will assume that the PDEs are uniformly distributed in both the soma and the dendrite. Thus, the concentration in the circle C_1 and in the rectangle C_2 obey the diffusion equation with a homogeneous degradation rate β,

$$\frac{\partial C_1(r,\theta,t)}{\partial t} = D\nabla^2 C_1 - \beta C_1, \quad (0 \le r \le R, -\pi \le \theta \le \pi), \tag{2}$$

$$\frac{\partial C_2(x,y,t)}{\partial t} = D\nabla^2 C_2 - \beta C_2, \quad (0 \le x \le L, -w \le y \le w), \tag{3}$$

where D is the diffusion constant of cAMP and where we have used a Cartesian coordinate system for the dendrite and a polar coordinate system for the soma.

It has been shown that the cAMP production machinery is distributed on both the soma and the dendrite membrane with little [7,8] to no [9] observable spatial heterogeneity. Thus, it is reasonable to assume that the neuron has a constant cAMP source flux, f with unit $1/(\mathrm{s}\ \mu\mathrm{m})$, on the entire membrane. Therefore, the boundary conditions on the various parts of the membrane read as

$$\frac{\partial C_1(R,\theta,t)}{\partial r} = \frac{f}{D}, \quad (\theta_0 \le \theta \le 2\pi - \theta_0), \tag{4}$$

$$\frac{\partial C_2(L,y,t)}{\partial x} = \frac{f}{D}, \quad (-w \le y \le w), \tag{5}$$

$$\frac{\partial C_2(x, \pm w,t)}{\partial y} = \pm \frac{f}{D}, \quad (0 \le x \le L). \tag{6}$$

We require that the concentration at the connection between the soma and the dendrite is continuous. Thus, under the condition that $w \ll R$, we have

$$C_1(R,\theta,t) = C_2(0,y,t), \quad (-\theta_0 < \theta < \theta_0), \tag{7}$$

$$\frac{\partial C_1(R,\theta,t)}{\partial r} = \frac{\partial C_2(0,y,t)}{\partial x}, \quad (-\theta_0 < \theta < \theta_0), \tag{8}$$

where $y \simeq R\theta$.

III. RESULTS

We will focus here on steady-state solutions, which can be found by setting the left-hand sides of Eqs. (2) and (3) to zero. Then, general steady-state solutions for $C_1(r,\theta)$ and $C_2(x,y)$ can be obtained as

$$C_1(r,\theta) = \sum_{m=0}^{\infty} B_m \frac{I_m(r/l)}{I'_m(R/l)} \cos m\theta + \frac{f}{\sqrt{\beta D}} \frac{\pi - \theta_0}{\pi} \frac{I_0(r/l)}{I'_0(R/l)} - \sum_{n=1}^{\infty} \frac{2f}{\sqrt{\beta D}} \frac{\sin n\theta_0}{n\pi} \frac{I_n(r/l)}{I'_n(R/l)} \cos n\theta, \tag{9}$$

$$C_2(x,y) = \sum_{n=0}^{\infty} A_n [e^{x\sqrt{(1/l)^2+(n\pi/w)^2}} + e^{(2L-x)\sqrt{(1/l)^2+(n\pi/w)^2}}] \times \cos\left(n\pi\frac{\theta}{\theta_0}\right) + \frac{f}{\sqrt{\beta D}} \frac{\cosh(x/l)}{\sinh(L/l)} + \frac{f}{\sqrt{\beta D}} \frac{\cosh(y/l)}{\sinh(w/l)}, \tag{10}$$

where $l = \sqrt{\frac{D}{\beta}}$ is a decay length. Here, and in the remainder of the paper, I_n represents the modified Bessel function of the first kind, and $'$ represents the derivative of the argument. The coefficients B_m are determined by A_n through Eq. (8),

$$B_0 = \frac{l}{2\pi} \int_{-\theta_0}^{\theta_0} g(\theta) d\theta, \tag{11}$$

$$B_m = \frac{l}{\pi} \int_{-\theta_0}^{\theta_0} g(\theta) d\theta, \quad m = 1,2,3, \ldots, \tag{12}$$

where function $g(\theta)$ is the gradient at the connection of the circle and the rectangle, i.e., a function of A_n, for $-\theta_0 < \theta < \theta_0$

$$g(\theta) = \frac{\partial C_2(0,y)}{\partial x} = \sum_{n=0}^{\infty} A_n \sqrt{\left(\frac{1}{l}\right)^2 + \left(\frac{n\pi}{w}\right)^2} \times [1 - e^{2L\sqrt{(1/l)^2+(n\pi/w)^2}}] \cos\left(n\pi\frac{\theta}{\theta_0}\right). \tag{13}$$

To determine A_n, we can apply the continuity condition (7), which results in a set of countable infinite linear equations for A_n: $MA = a$, where M and a are a matrix and column vector with infinite dimension determined by Eq. (7), respectively, and where A is the vector $A_0, A_1, \ldots$.

The resulting linear algebra problem is difficult to solve, even numerically. Fortunately, as we will see below, for thin dendrites the series converges rapidly and the first coefficient A_0 can be calculated in the limit $w = \theta_0 \to 0$. Let us use $c_{1,2}$ to represent the concentrations for this limiting case, which can be related to $C_{1,2}$ respectively, as follows:

$$c_1(r,\theta) = \lim_{\theta_0 \to 0} C_1(r,\theta), \tag{14}$$

$$c_2(x) = \lim_{w\to 0} \int_{-w}^{w} C_2(x,y)dy. \tag{15}$$

The diffusion equation and boundary condition for c_1 are identical to Eqs. (2) and (4), while the diffusion equation for c_2 becomes one dimensional,

$$0 = D\frac{d^2c_2}{dx^2} - \beta c_2 + 2f, \tag{16}$$

with as boundary condition

$$\frac{dc_2(L)}{dx} = \lim_{w\to 0} \int_{-w}^{w} \frac{f}{D} dw = 0. \tag{17}$$

The continuity equations (7) and (8) at the junction of the dendrite and the soma reduces to

$$c_2(0) = \lim_{\theta_0\to 0} \int_{-\theta_0}^{\theta_0} Rc_1(R,\theta)d\theta = 0, \tag{18}$$

$$\frac{\partial c_1(R)}{\partial r} = \frac{f}{D} + \frac{J}{DR}\delta(\theta), \tag{19}$$

$$\frac{dc_2(0)}{dx} = \frac{J}{D}, \tag{20}$$

where J denotes the flux from the dendrite to the soma with units $1/s$. The proof of the last identity in Eq. (18) is given in Appendix A. $c_2(0)=0$ reflects the fact that in this extreme case, molecules at the junction flow into the soma and never flow back to the dendrite. Solving the above equations leads to an analytic expression

$$J = 2fl\tanh(L/l), \tag{21}$$

$$c_1(r,\theta) = \frac{f}{\sqrt{\beta D}}\frac{I_0(r/l)}{I_0'(R/l)} + \frac{f}{\beta R}\frac{\tanh(L/l)}{\pi}\frac{I_0(r/l)}{I_0'(R/l)} + \frac{2f}{\beta R}\frac{\tanh(L/l)}{\pi}\sum_{n=1}^{\infty}\frac{I_n(r/l)}{I_n'(R/l)}\cos n\theta, \tag{22}$$

$$c_2(x) = \frac{2f}{\beta} - \frac{2f}{\beta}\frac{e^{x/l}}{1+e^{2L/l}} - \frac{2f}{\beta}\frac{e^{(2L-x)/l}}{1+e^{2L/l}}. \tag{23}$$

Comparing the coefficients of $c_{1,2}$ and $C_{1,2}$ through Eqs. (14) and (15), we find

$$A_0 = -\frac{f}{\beta w}\frac{1}{1+e^{2L/l}}, \tag{24}$$

$$B_0 = \frac{f}{\beta R}\frac{\tanh(L/l)}{\pi} + o(w), \tag{25}$$

$$B_m = \frac{2f}{\beta R}\frac{\tanh(L/l)}{\pi} + o(w), \quad m = 1,2,3,\ldots. \tag{26}$$

Therefore, we can obtain an approximate form of the concentration in the soma

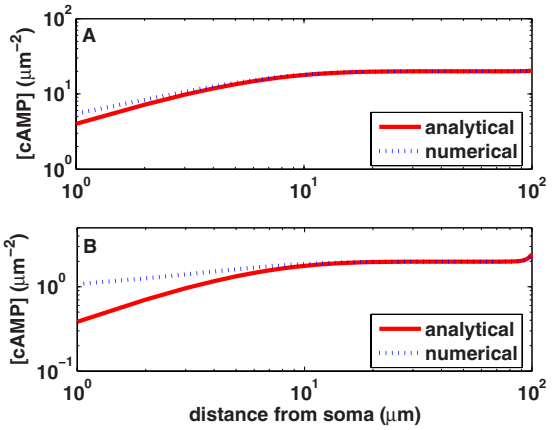

FIG. 2. (Color online) A comparison between the analytical approximation (solid line) and the numerical result (dotted line) for the cAMP concentration in the dendrite along the symmetry line for (a) $w=0.1$ μm and (b) $w=1$ μm. Other parameters used are $R=10$ μm, $L=100$ μm, $f=20/(\text{s}\,\mu\text{m})$, $D=200$ $\mu\text{m}^2/\text{s}$, $\beta=10$ s^{-1}.

$$C_1(r,\theta) = \sum_{n=1}^{\infty}\frac{2f}{\beta R}\frac{\tanh(L/l)}{\pi}\frac{I_n(r/l)}{I_n'(R/l)}\cos n\theta - \sum_{n=1}^{\infty}\frac{2f}{\sqrt{\beta D}}\frac{\sin n\theta_0}{n\pi}\frac{I_n(r/l)}{I_n'(R/l)}\cos n\theta + \frac{f}{\beta R}\frac{\tanh(L/l)}{\pi}\frac{I_0(r/l)}{I_0'(R/l)} + \frac{f}{\sqrt{\beta D}}\frac{\pi-\theta_0}{\pi}\frac{I_0(r/l)}{I_0'(R/l)} + o(w), \tag{27}$$

and in the dendrite

$$C_2(x,0) = \frac{f}{\sqrt{\beta D}}\frac{\cosh(x/l)}{\sinh(L/l)} + \frac{f}{\sqrt{\beta D}}\frac{1}{\sinh(w/l)} - \frac{f}{\beta w}\frac{\cosh[(L-x)/l]}{\cosh(L/l)} + o\left(\frac{1}{w}\right). \tag{28}$$

Furthermore the gradient at the junction reads in this limit

$$\frac{\partial C_2(0,0)}{\partial x} = \frac{f}{w\sqrt{\beta D}}\tanh(L/l) + o\left(\frac{1}{w}\right). \tag{29}$$

In Fig. 2 we plot the approximate solution in the dendrite as a function x (solid line), along with the full solution obtained by numerically solving the model (dotted line) for two different dendrite widths. As we can see, the approximate concentration is quite close to the numerical solution away from the soma but starts to deviate closer to the soma. The analytical solution is a function of w, of course, and approaches the numerical solution as w get smaller. This is also demonstrated in Fig. 3(a), where we plot the gradient at the junction of the soma and the dendrite for both the full solution (circles) and our analytical approximation (solid line). Clearly, the error between the two results plotted in Fig. 3(b) becomes smaller as the width of the dendrite decreases, consistent with the expectation that the analytical solution converges to the full solution as $w\to 0$. We note here that our

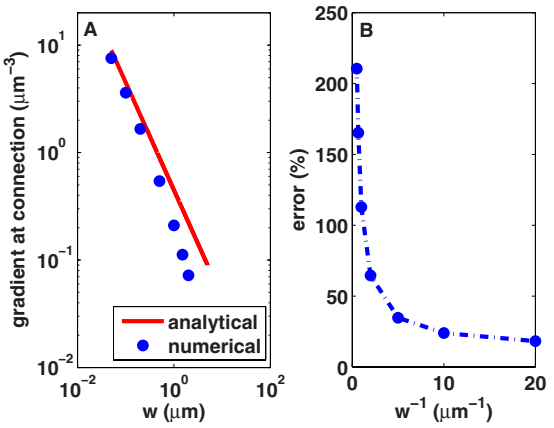

FIG. 3. (Color online) (A) A comparison between the analytical approximation (solid line) and the numerical result (circles) for the gradient at soma-dendrite junction as a function of w. (B) The corresponding error as a function of w^{-1}. Other parameters used are $R=10$ μm, $L=100$ μm, $f=20/(\text{s}\ \mu\text{m})$, $D=200$ $\mu\text{m}^2/\text{s}$, $\beta=10\text{s}^{-1}$.

FIG. 4. (Color online) Numerical results without degradation mechanism for different widths of the dendrite $w=0.5,1.0,1.5,2.0$ μm (from left to right, respectively). The radius of the soma was taken to be $R=10$ μm and the length of the dendrite was chosen to be $L=100$ μm. Other parameters are $f=20/(\text{s}\ \mu\text{m})$, $D=200$ $\mu\text{m}^2/\text{s}$, $T=300$ s.

results can be extended to three dimensions as shown in Appendix B.

IV. DISCUSSION

The main advantage of having analytical expressions for the concentrations in the two compartments and the concentration gradient at the junction is that it becomes easier to assess the effect of the system parameters on compartmentalization. From Eq. (27), we see that the concentration at the center of the soma can be approximated by

$$C_1(0,0) \simeq \frac{f}{I_0'(R/l)}\left(\frac{\tanh(L/l)}{\beta\pi R}+\frac{1}{\sqrt{\beta D}}\right). \tag{30}$$

Upon inspection of this equation, we can conclude that the cAMP concentration in the soma is largely independent of the length of the dendrite provided that this length is much larger that the decay length l. Furthermore, the concentration is independent of the width of the dendrite and, thus, for small w and $L \gg l$, the soma concentration depends only weakly on the geometry of the dendrite and is mostly determined by the degradation rate β.

A similar analysis can be carried out for the concentration in the middle of the dendrite ($x=L/2$), where we find from Eq. (28),

$$C_2(L/2,0) \simeq \frac{f}{\beta w}\left(1-\frac{\cosh[L/(2l)]}{\cosh(L/l)}\right)+\frac{f}{\sqrt{\beta D}}\frac{\cosh[L/(2l)]}{\sinh(L/l)}. \tag{31}$$

Thus, the cAMP level in dendrite decreases as the degradation rate increases but is also strongly dependent on the width of the dendrite. We note that for $L \gg l$ the concentration reduces to the simple form $C_2(L/2,0) \simeq \frac{f}{\beta w}$. We can also conclude that the largest gradient of cAMP occurs at the junction between the soma and the dendrite and Eq. (29) shows that this gradient is inversely proportional to w and to the square root of the diffusion constant and the degradation rate. It also shows that the radius of cell body has no effect on the gradient. In fact, for $L \gg l$ the gradient becomes independent of the length of the dendrite and the only geometric dependence is through the width $\frac{\partial C_2(0,0)}{\partial x} \simeq \frac{f}{w\sqrt{\beta D}}$.

Finally, we have performed numerical simulations, using MATLAB's PDE Toolbox, to confirm the role of degradation and geometry on the concentration fields in the soma and dendrite. Figure 4 shows the cAMP concentration in a color scale in the absence of degradation ($\beta=0$) using $C_1(r,\theta)=C_2(x,y)=0$ as initial condition. Clearly, this is an unrealistic situation as the concentration would increase indefinitely as long as the flux is constant. Nevertheless, we can investigate the dependence of the cAMP fields in the two compartments by plotting the concentration at a particular time. This is done in Fig. 4 for four different values of w and $T=300$ s. We can see that the concentration in the dendrite increases significantly if the width becomes smaller. However, in support of our analysis above, the concentration in the soma increases as well and the resulting high concentration in both the soma and the dendrite would make it difficult to achieve signal specificity. In Fig. 5, we show the steady-state cAMP concentration for the same set of dendrite widths and a nonzero degradation constant. Again, the results are shown for $T=300$ s, chosen such that the concentration has reached a steady state, starting at the same initial condition as in Fig. 4. As is evident from the figures, the introduction of cAMP degradation is able to drastically reduce the concentration of cAMP in the soma while maintaining a high cAMP level in thin dendrites. The results also show that w has little effect on cAMP level in the soma, again verifying our analytic results above.

In summary, we have derived analytical solutions for the cAMP concentration field in a simplified neuronal geometry, where the difference in surface-to-volume ratio between the soma and the dendrite, coupled with a constant cAMP flux, leads to compartmentalization [6]. We find that the expression becomes particularly easy to analyze in the limit of thin

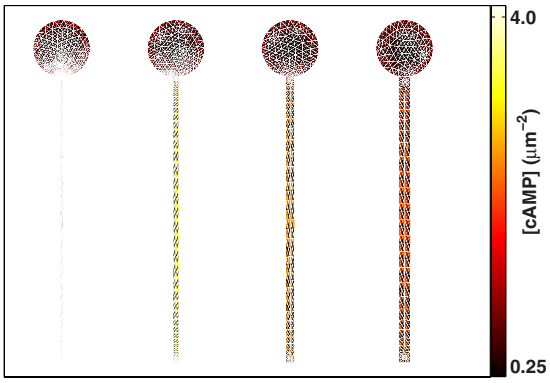

FIG. 5. (Color online) Numerical results with degradation rate $\beta=10\ s^{-1}$ for different widths of the dendrite $w=0.5,1.0,1.5,2.0\ \mu$m (from left to right, respectively). Parameter values are as in Fig. 4.

dendrites. Our solutions show that a sufficient level of degradation, along with a dendrite with a width that is much smaller than the radius of the soma, does lead to cAMP compartmentalization and offers a mechanism for signal specificity.

ACKNOWLEDGMENT

This work was supported by the Center for Theoretical Biological Physics (Grant No. NSF PHY-0822283).

APPENDIX A: PROOF OF EQ. (18)

Here, we will present a proof of the last identity in Eq. (18) $\lim_{\theta_0\to 0}\int_{-\theta_0}^{\theta_0} Rc_1(R,\theta)d\theta=0$. From Eq. (2) with the left-hand side set to zero and the boundary condition (19), we can obtain the general solution for c_1 at the junction $-\theta_0<\theta<\theta_0$

$$c_1(R,\theta)=\left[\frac{f}{\sqrt{\beta D}}+\frac{1}{2\pi}\frac{J}{\sqrt{\beta DR}}\right]\frac{I_0(R/l)}{I_0'(R/l)}+\frac{1}{\pi}\frac{f}{D}\sum_{n=1}^{\infty}\frac{I_n(R/l)}{(R/l)I_n'(R/l)}\cos n\theta, \tag{A1}$$

where J is an unknown constant. The first term of $c_1(R,\theta)$ is independent of θ, so the limit of the first term's integration gives zero. Thus, we need to prove $\lim_{\theta_0\to 0} Q(\theta_0)=0$, where $Q(\theta_0)=\int_{-\theta_0}^{\theta_0}\sum_{n=1}^{\infty}\frac{I_n(R/l)}{(R/l)I_n'(R/l)}\cos n\theta d\theta$. Since we cannot change the order of the integral with the infinite summation, we will find the upper and lower bounds of $Q(\theta_0)$ instead. It is easy to show that for positive arguments x

$$\frac{n+1}{n(n+1)+\frac{x^2}{2}}<\frac{I_n(x)}{xI_n'(x)}<\frac{1}{n},\quad n=1,2,3,\ldots. \tag{A2}$$

Thus, we have

$$\begin{aligned}\left|\frac{I_n(x)}{xI_n'(x)}\cos n\theta-\frac{\cos n\theta}{n}\right| &\le \left|\frac{I_n(x)}{xI_n'(x)}-\frac{1}{n}\right||\cos n\theta| \\ &\le \left|\frac{I_n(x)}{xI_n'(x)}-\frac{1}{n}\right| \\ &= \frac{1}{n}-\frac{I_n(x)}{xI_n'(x)}<\frac{1}{n}-\frac{n+1}{n(n+1)+\frac{x^2}{2}} \\ &= \frac{x^2}{2}\frac{1}{(n+1)n^2+\frac{x^2}{2}n}<\frac{x^2}{2}\frac{1}{(n+1)n^2}.\end{aligned} \tag{A3}$$

Therefore, for each n, $\frac{I_n(x)}{xI_n'(x)}\cos n\theta$ is bounded as follows:

$$\frac{\cos n\theta}{n}-\frac{x^2}{2}\frac{1}{(n+1)n^2}<\frac{I_n(x)}{xI_n'(x)}\cos n\theta<\frac{\cos n\theta}{n}+\frac{x^2}{2}\frac{1}{(n+1)n^2}. \tag{A4}$$

Thus, the upper and lower bounds of the infinite summation is given by

$$\sum_{n=1}^{\infty}\frac{\cos n\theta}{n}\pm\frac{1}{2}\left(\frac{R}{l}\right)^2\sum_{n=1}^{\infty}\frac{1}{(n+1)n^2}=\frac{1}{2}\log\frac{1}{2-2\cos\theta}\pm\frac{1}{2}\left(\frac{R}{l}\right)^2\left(\frac{\pi^2}{6}-1\right). \tag{A5}$$

By integrating Eq. (A5) from $-\theta_0$ to θ_0, we find the upper and lower bounds of $Q(\theta_0)$

$$i[Li_2(e^{-i\theta_0})-Li_2(e^{i\theta_0})]-\left(\frac{R}{l}\right)^2\left(\frac{\pi^2}{6}-1\right)\theta_0<Q(\theta_0)<i[Li_2(e^{-i\theta_0})-Li_2(e^{i\theta_0})]+\left(\frac{R}{l}\right)^2\left(\frac{\pi^2}{6}-1\right)\theta_0, \tag{A6}$$

where Li_2 denotes the dilogarithm function. Taking the limit of $\theta_0\to 0$ in Eq. (A6), both the lower and upper bounds go to zero, so that $\lim_{\theta_0\to 0} Q(\theta_0)=0$ and, hence, $\lim_{\theta_0\to 0}\int_{-\theta_0}^{\theta_0} Rc_1(R,\theta)d\theta=0$.

APPENDIX B: SOLUTIONS FOR 3D

The analytic solutions found in two dimensions can be extended to a three-dimensional geometry. By rotating Fig. 1 around the x axis, we can arrive at a 3D model with the cell body as a sphere with radius R, and the dendrite as a cylinder with length L and radius w. Since the dendrite is very thin compared to the soma, i.e., $w\ll R$, Eq. (1) remains valid. The concentration in the sphere $\hat{C}_1(r,\theta,\varphi)$ and in the cylinder $\hat{C}_2(x,\rho,\varphi)$ obey the diffusion equation with a homogeneous degradation rate β as in Eqs. (2) and (3), but now written in n spherical and cylinder coordinates, respectively, where

$0 \le r \le R$, $0 \le \theta \le \pi$, $0 \le x \le L$, $0 \le \rho \le w$, and $0 \le \varphi \le 2\pi$. Because of the symmetry around x axis, both concentration fields are independent of φ and they become effectively two dimensional: $\hat{C}_1(r,\theta,\varphi) = \hat{C}_1(r,\theta)$ and $\hat{C}_2(x,\rho,\varphi) = \hat{C}_2(x,\rho)$.

In the 3D case, the constant cAMP source flux F has units of $1/(\mathrm{s}\ \mu\mathrm{m}^2)$, and the boundary conditions read as

$$\frac{\partial \hat{C}_1(R,\theta)}{\partial r} = \frac{F}{D}, \quad (\theta_0 \le \theta \le \pi, 0 \le \varphi \le 2\pi), \tag{B1}$$

$$\frac{\partial \hat{C}_2(L,\rho)}{\partial x} = \frac{F}{D}, \quad (0 \le \rho \le w, 0 \le \varphi \le 2\pi), \tag{B2}$$

$$\frac{\partial \hat{C}_2(x,w)}{\partial \rho} = \frac{F}{D}, \quad (0 \le x \le L, 0 \le \varphi \le 2\pi). \tag{B3}$$

Since $w \ll R$, we can approximate the junction of the sphere and the cylinder to be a disk, and we require that the concentration and gradient at the dist to be continuous

$$\hat{C}_1(R,\theta) = \hat{C}_2(0,\rho), \quad (0 \le \theta < \theta_0, 0 \le \varphi \le 2\pi), \tag{B4}$$

$$\frac{\partial \hat{C}_1(R,\theta)}{\partial r} = \frac{\partial \hat{C}_2(0,\rho)}{\partial x}, \quad (0 \le \theta < \theta_0, 0 \le \varphi \le 2\pi), \tag{B5}$$

where $\rho \simeq R\theta$.

Therefore, the steady-state solution can be obtained as

$$\begin{aligned}\hat{C}_1(r,\theta) = {} & \sum_{m=0}^{\infty} \hat{B}_m \frac{i_m(r/l)}{i_m'(R/l)} p_m(\cos\theta) + \frac{F}{\sqrt{\beta D}} \frac{1+\cos\theta_0}{2} \frac{i_0(r/l)}{i_0'(R/l)} \\ & + \sum_{n=1}^{\infty} \frac{F}{\sqrt{\beta D}} \frac{1}{2} [p_{n+1}(\cos\theta_0) \\ & - p_{n-1}(\cos\theta_0)] \frac{i_n(r/l)}{i_n'(R/l)} p_n(\cos\theta),\end{aligned} \tag{B6}$$

$$\begin{aligned}\hat{C}_2(x,\rho) = {} & \sum_{n=0}^{\infty} \hat{A}_n [e^{x\sqrt{(1/l)^2+k_n^2}} + e^{(2L-x)\sqrt{(1/l)^2+k_n^2}}] J_0(k_n\rho) \\ & + \frac{F}{\sqrt{\beta D}} \frac{\cosh(x/l)}{\sinh(L/l)} + \frac{F}{\sqrt{\beta D}} \frac{I_0(\rho/l)}{I_0'(w/l)},\end{aligned} \tag{B7}$$

where i_n and J_n represent the modified spherical Bessel function of the first kind and Bessel function of the first kind, respectively, k_n is the nth root of $J_1(k_n w) = 0$, and P_n^m denotes the Legendre function. Here $p_n = P_n^0$. The coefficients $\hat{B}_m$ are determined by $\hat{A}_n$ through Eq. (B5),

$$\hat{B}_m = \frac{2m+1}{2} l \int_0^{\theta_0} \hat{g}(\theta) p_m(\cos\theta) \sin\theta d\theta, \quad m = 0,1,2,\ldots, \tag{B8}$$

where $\hat{g}(\theta)$ is the flux from the dendrite to the soma, given by

$$\begin{aligned}\hat{g}(\theta) = {} & \frac{\partial \hat{C}_2(0,\rho)}{\partial x} \\ = {} & \sum_{n=0}^{\infty} \hat{A}_n \sqrt{\left(\frac{1}{l}\right)^2 + k_n^2} [1 - e^{2L\sqrt{(1/l)^2+k_n^2}}] J_0(k_n\rho).\end{aligned} \tag{B9}$$

To determine $\hat{A}_n$, one needs to solve Eq. (B4), which is a difficult task.

Similarly to our two-dimensional case, we can consider the limiting case $w = \theta_0 = 0$, i.e., a sphere connected to a line. We use $\hat{c}_{1,2}$ to represent the concentrations for this limit case, which can be related to $\hat{C}_{1,2}$ as follows:

$$\hat{c}_1(r,\theta) = \lim_{\theta_0 \to 0} \hat{C}_1(r,\theta), \tag{B10}$$

$$\hat{c}_2(x) = \lim_{w \to 0} \int_0^{2\pi} \int_0^{w} \hat{C}_2(x,\rho) d\rho d\varphi. \tag{B11}$$

The diffusion equation and boundary condition for $\hat{c}_1$ are identical to Eqs. (2) and (B1), while the diffusion equation for $\hat{c}_2$ becomes one dimensional

$$0 = D \frac{d^2 \hat{c}_2}{dx^2} - \beta \hat{c}_2 + 2f, \tag{B12}$$

where $f = \pi w F$. The boundary condition is

$$\begin{aligned}\frac{d\hat{c}_2(L)}{dx} = {} & \lim_{w \to 0} \int_0^{2\pi} \int_0^{w} \frac{F}{D} \rho d\rho d\varphi \\ = {} & \lim_{w \to 0} \int_0^{2\pi} \int_0^{w} \frac{f}{\pi w D} \rho d\rho d\varphi = 0\end{aligned} \tag{B13}$$

and the continuity property at the junction reduces to

$$\hat{c}_2(0) = \lim_{\theta_0 \to 0} \int_0^{2\pi} \int_0^{\theta_0} R^2 \sin\theta \hat{c}_1(R,\theta) d\theta d\varphi = 0, \tag{B14}$$

$$\frac{\partial \hat{c}_1(R)}{\partial r} = \frac{f}{\pi w D} + \frac{J}{D R^2} \delta^2(\theta,\varphi), \tag{B15}$$

$$\frac{d\hat{c}_2(0)}{dx} = \frac{J}{D}, \tag{B16}$$

where $\delta^2(\theta,\varphi)$ denotes the Dirac delta function in spherical coordinates. Solving the above equations leads to an analytic solution

$$J = 2fl \tanh(L/l), \tag{B17}$$

$$\begin{aligned}\hat{c}_1(r,\theta) = {} & \frac{f}{\beta R^2} \frac{\tanh(L/l)}{\pi} \sum_{n=0}^{\infty} (2n+1) \frac{i_n(r/l)}{i_n'(R/l)} p_n(\theta) \\ & + \frac{f}{\pi w \sqrt{\beta D}} \frac{i_0(r/l)}{i_0'(R/l)},\end{aligned} \tag{B18}$$

$$\hat{c}_2(x) = \frac{2f}{\beta} - \frac{2f}{\beta}\frac{e^{x/l}}{1+e^{2L/l}} - \frac{2f}{\beta}\frac{e^{(2L-x)/l}}{1+e^{2L/l}}. \tag{B19}$$

Comparing the coefficients of $\hat{c}_{1,2}$ with those of $\hat{C}_{1,2}$ through Eqs. (B10) and (B11), we find

$$\hat{A}_0 = -\frac{F}{\beta w}\frac{1}{1+e^{2L/l}},$$

$$\hat{B}_m = (2m+1)\frac{\pi w F}{\beta R^2}\tanh(L/l) + o(w^2), \tag{B20}$$

$$m = 0,1,2,\ldots. \tag{B21}$$

Therefore, we can obtain an approximate form for the concentration in the soma

$$\hat{C}_1(r,\theta) = \frac{\pi w F}{\beta R^2}\tanh(L/l)\sum_{n=0}^{\infty}(2n+1)\frac{i_n(r/l)}{i_n'(R/l)}p_n(\cos\theta) + \frac{F}{2\sqrt{\beta D}}\sum_{n=1}^{\infty}[p_{n+1}(\cos\theta_0) - p_{n-1}(\cos\theta_0)]\frac{i_n(r/l)}{i_n'(R/l)}p_n(\cos\theta) + \frac{F}{\sqrt{\beta D}}\frac{1+\cos\theta_0}{2}\frac{i_0(r/l)}{i_0'(R/l)} + o(w^2), \tag{B22}$$

and in the dendrite

$$\hat{C}_2(x,0) = \frac{F}{\sqrt{\beta D}}\frac{\cosh(x/l)}{\sinh(L/l)} + \frac{F}{\sqrt{\beta D}}\frac{1}{I_0'(w/l)} - \frac{F}{\beta w}\frac{\cosh[(L-x)/l]}{\cosh(L/l)} + o\left(\frac{1}{w}\right). \tag{B23}$$

Furthermore, the gradient at the junction reads in this limit as

$$\frac{\partial \hat{C}_2(0,0)}{\partial x} = \frac{F}{w\sqrt{\beta D}}\tanh(L/l) + o\left(\frac{1}{w}\right), \tag{B24}$$

similar in form to the two-dimensional case.

[1] I. L. Buxton and L. L. Brunton, J. Biol. Chem. **258**, 10233 (1983).

[2] M. Zaccolo and T. Pozzan, Science **295**, 1711 (2002).

[3] T. C. Rich, K. A. Fagan, T. E. Tse, J. Schaack, D. M. Cooper, and J. W. Karpen, Proc. Natl. Acad. Sci. U.S.A. **98**, 13049 (2001).

[4] M. A. Davare, V. Avdonin, D. D. Hall, E. M. Peden, A. Burette, R. J. Weinberg, M. C. Horne, T. Hoshi, and J. W. Hell, Science **293**, 98 (2001).

[5] W. Chen, H. Levine, and W. Rappel, Phys. Biol. **5**, 1478 (2008).

[6] S. R. Neves, P. Tsokas, A. Sarkar, E. A. Grace, P. Rangamani, S. M. Taubenfeld, C. M. Alberini, J. C. Schaff, R. D. Blitzer, I. I. Moraru, and R. Iyengar, Cell **133**, 666 (2008).

[7] T. C. Rainbow, B. Parsons, and B. B. Wolfe, Proc. Natl. Acad. Sci. U.S.A. **81**, 1585 (1984).

[8] G. E. Duncan, K. Y. Little, P. A. Koplas, J. A. Kirkman, G. R. Breese, and W. E. Stumpf, Brain Res. **561**, 84 (1991).

[9] G. A. Ordway, C. Gambarana, and A. Frazer, J. Pharmacol. Exp. Ther. **247**, 379 (1988).